Earth and Planetary Science Letters 337–338 (2012) 93–103

Contents lists available at SciVerse ScienceDirect

Earth and Planetary Science Letters

journal homepage: www.elsevier.com/locate/epsl

Magnetic fidelity of lunar samples and implications for an ancient core dynamo

Sonia M. Tikoo*, Benjamin P. Weiss, Jennifer Buz, Eduardo A. Lima, Erin K. Shea, Gabriela Melo, Timothy L. Grove

Department of Earth, Atmospheric, and Planetary Sciences, Massachusetts Institute of Technology, Cambridge, MA, USA

ARTICLE INFO

Article history:
Received 25 November 2011
Received in revised form
4 May 2012
Accepted 20 May 2012
Available online 21 June 2012

Keywords:
lunar paleomagnetism
AF demagnetization
paleointensity
lunar dynamo
anhysteretic remanence
magnetic anisotropy

ABSTRACT

Some lunar rocks have stable magnetizations that provide compelling evidence for an ancient lunar core dynamo. However, a longstanding problem has been interpreting the unstable alternating field (AF) demagnetization behavior observed in the remaining majority of the Apollo lunar sample suite. Similar unstable behavior has also been observed for many meteorites. It is unclear whether the behavior of these samples indicates that they formed in the absence of an ancient magnetizing field or whether they simply have poor magnetic recording properties. It is necessary to distinguish between these two possibilities in order to determine whether paleomagnetic fields were present on a sample's parent body. To address this issue, we analyzed five samples whose rock magnetic properties span the full suite of observed demagnetization behaviors: mare basalts 15556, 15016, 12017, 10020, and troctolite 76535. We demonstrate that the effects of spurious anhysteretic remanent magnetization (ARM) during AF demagnetization, in combination with multidomain magnetic carriers and magnetic remanence anisotropy, are likely responsible for the apparently poor magnetic behavior of many lunar samples. Therefore, the unstable AF demagnetization behavior observed for many lunar samples is not alone sufficient for ruling out the presence of an ancient lunar core dynamo. Nevertheless, spurious ARM may explain the observation of surprisingly high (≥ 1 μT) Apollo-era paleointensity measurements for samples thought to have formed after the cessation of a lunar core dynamo (< 1.5 Ga).

1. Introduction

A central question in lunar science is whether the Moon fully differentiated and formed a liquid metallic core. Moment of inertia data (Konopliv et al., 1998) and the lunar induced magnetic dipole moment (Hood et al., 1999) support the existence of a 220–450 km radius iron core, while Apollo seismic data provide evidence for a 240 km radius solid inner core (Weber et al., 2011), surrounded by a 330–365 km radius liquid outer core (Garcia et al., 2010; Weber et al., 2011). Magnetic studies provide another means to test for a lunar core through the identification of a paleomagnetic field: the detection of remanent magnetization in the lunar crust (Dyal et al., 1970) and in returned Apollo samples (Fuller and Cisowski, 1987) indicate that the Moon may have once possessed a dynamo magnetic field and, by implication, a molten, advecting metallic core (Garrick-Bethell et al., 2009; Shea et al., 2012). The existence of an ancient lunar dynamo is broadly consistent with a high-temperature lunar origin (Pritchard and Stevenson, 2000; Runcorn, 1996). It also would have implications for the physics of dynamo generation because a prolonged and strong lunar field may require nontraditional power sources (Dwyer et al., 2011; Le Bars et al., 2011; Wieczorek et al., 2006; Wieczorek et al., 2012).

Although it has been known for decades that lunar rocks are magnetized, only recent studies have clearly determined that the magnetizing fields resulted from a core dynamo rather than from other field-generating mechanisms. In particular, a key proposed alternative to the core dynamo hypothesis is that lunar paleofields were transiently produced or amplified by currents in meteoroid impact-generated plasmas (Hood and Artemieva, 2008; Srnka, 1977). To address this ambiguity, Garrick-Bethell et al. (2009) and Shea et al. (2012) analyzed the paleomagnetism of samples unlikely to have recorded any impact-generated fields, the 4.2 billion year old (Ga) lunar troctolite 76535 and the 3.7 Ga mare basalt 10020. These rocks cooled from their Curie points to ambient temperatures over timescales greatly exceeding the expected duration of even the longest lived impact-generated magnetic fields (lasting ~1 day) (Garrick-Bethell et al., 2009). These samples exhibit no petrographic evidence for shock effects (peak pressures < 5 GPa), demonstrating that they are unlikely to have recorded transient magnetic fields via the shock remanent

* Correspondence to: 77 Massachusetts Avenue 54–825, Cambridge, MA 02139, USA. Tel.: +1 617 324 3935; fax: +1 617 258 7401.
E-mail address: smtikoo@mit.edu (S.M. Tikoo).

0012-821X/$ - see front matter © 2012 Elsevier B.V. All rights reserved.
http://dx.doi.org/10.1016/j.epsl.2012.05.024

magnetization (SRM) process. Both samples contain a natural remanent magnetization (NRM) with a high coercivity component that is unidirectional across mutually oriented subsamples and which monotonically decays to the origin during demagnetization experiments (Garrick-Bethell et al., 2010; Shea et al., 2012). The stable magnetization components of 76535 and 10020 were acquired in fields of at least 1 μT and probably several tens of μT (Garrick-Bethell et al., 2010; Shea et al., 2012). The lower end of this range is consistent with the expected ~15–20 μT upper limit for surface fields from an ancient lunar dynamo operating in a small (~300–400 km radius) (Wieczorek et al., 2006; Dwyer et al., 2011; Le Bars et al., 2011). These data collectively suggest that the characteristic magnetization components in these samples are thermoremanent magnetization (TRM) obtained by cooling from the Curie point in the presence of a stable long-lived paleofield like that from a core dynamo.

The problem addressed in the present study is that the stable NRMs of 76535 and 10020 are exceptional when compared to other lunar samples. Most lunar rocks subjected to paleomagnetic studies display low fidelity NRM behavior during alternating field (AF) demagnetization experiments, characterized by non-monotonic decline of magnetization intensity and rapidly varying magnetization directions (Brecher, 1976; Hoffman and Banerjee, 1975). Such behavior makes it difficult to determine whether the observed magnetization was acquired in the presence or absence of a core dynamo field. The AF demagnetization procedure itself has been proposed to be responsible for much of this behavior. A frequent problem is that samples acquire spurious (i.e., unintended) anhysteretic remanent magnetization (ARM), which manifests as unstable moment directions and non-monotonic changes in NRM intensity during a series of AF steps [see Fig. 1 of Weiss et al. (2010)]. Another less common problem which may result in poor AF demagnetization behavior is the acquisition of gyroremanent magnetization (GRM) (Hu et al., 1998; Stephenson, 1980, 1993). GRM is a laboratory-produced component specific to single-domain-like particles that is acquired perpendicularly to the preferred easy axis orientation as well as to the axis of the last AF application (Dunlop and Ozdemir, 1997) and grows monotonically with peak AC field during AF demagnetization [see Fig. S5 of Garrick-Bethell et al. (2009)].

ARM noise is generated by the presence of even harmonics in the AF waveform during demagnetization (Collinson, 1983) due to harmonic distortion in oscillator and amplifier stages or spurious waveforms appearing at non-harmonic frequencies caused by interference (Figs. 1a, S1, and S2). The sum of the fundamental wave and the second harmonic or another contaminating frequency often creates asymmetry of the positive and negative peak values of the waveform, leading to the acquisition of ARM (see Supplementary material). This unintended ARM can be acquired along all three orthogonal axes by grains with coercivities up to that of the peak AC field of the AF step. Depending on the stability of the AF waveform spectrum, repeat AF applications at the same peak AC field may produce scatter in the NRM direction, suggesting that spurious ARM results from noise in the AF waveform and is not readily predictable. The magnitude of spurious ARM typically increases with AF amplitude because the magnitude of the second harmonic itself increases with AF amplitude.

Kamacite- and taenite-bearing materials like lunar rocks and many meteorites are primarily multidomain due to the small single domain stability range of these minerals. Spurious ARM is especially problematic for multidomain samples because they are dominated by low coercivity grains (e.g. Nagata et al., 1973; Weiss et al., 2010): as demagnetization proceeds to higher AF amplitudes, the magnitude of the primary magnetization in the sample decreases while the net moment becomes increasingly overpowered by spurious ARM acquired by low-coercivity grains (Fig. 1b). On the other hand, spurious ARM is much less of a problem in terrestrial paleomagnetic studies because iron oxides like magnetite and hematite much more commonly form pseudo single domain and smaller grains. The lack of noticeable adverse effects caused by nonideal AF demagnetization in terrestrial samples likely accounts for why the full implications of spurious ARM for paleomagnetic studies have not been previously appreciated.

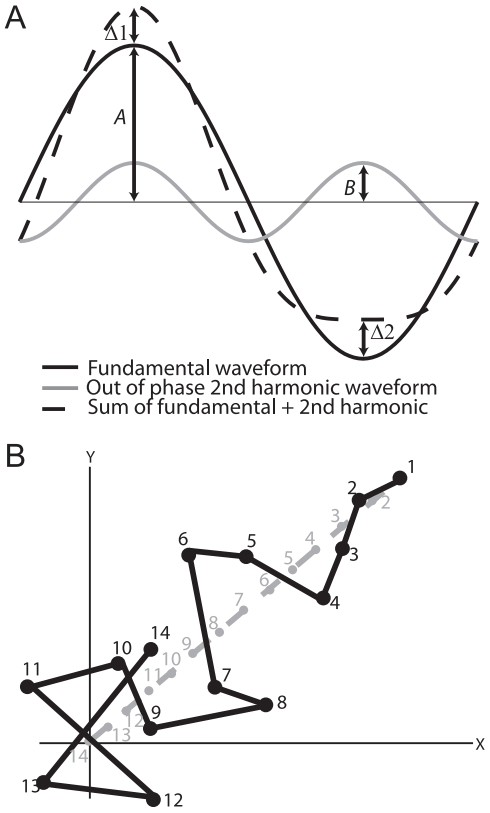

Fig. 1. Cause and effects of spurious ARM. (A) Generation of spurious ARM as a result of the summation of the fundamental AF waveform component of amplitude A with its second harmonic of amplitude B. Modified from Collinson (1983). Δ1 represents the increase in amplitude of the positive peak whereas Δ2 represents the increase in amplitude of the negative peak. Note that for a fixed amplitude ratio A/B between the harmonics, Δ1 and Δ2 are proportional to A (for the relative phases depicted here, Δ1 and Δ2 are in fact equal to the amplitude of the second harmonic; for other cases see Fig. S1). Therefore, the effective bias field changes for each period during the ramp-down of an AF application. (B) Schematic effects of spurious ARM on a theoretical AF demagnetization. The light gray line and points show an ideal scenario of NRM being stepwise demagnetized with NRM trending toward the origin. The black line and points show AF demagnetization affected by spurious ARM acquired during demagnetization. Numbers next to data points correspond to AF steps during the demagnetization experiment.

Another related source of unstable AF demagnetization has been ascribed to "textural remanence" in which the NRM is controlled by magnetic anisotropy resulting from foliated or lineated magnetic fabrics in samples. Such fabrics may originate from shock or primary igneous processes. These effects can be dramatically expressed as pinning of the NRM vector during demagnetization (zig-zag demagnetization) along an axial direction or within a plane (Brecher, 1976, 1977; Hoffman and Banerjee, 1975).

Unstable demagnetization behavior, observed in many lunar samples as well as iron-bearing meteorites (Table S1), makes it difficult to pinpoint the origin of magnetization in these samples. Therefore, it is important to assess the magnetic recording fidelity of such samples before attempting to ascertain whether they

were formed in the presence or absence of a dynamo field. With this goal, we studied the AF demagnetization behavior and magnetic recording capacities of low fidelity mare basalts 15556, 15016, and 12017 which were previously observed to exhibit spurious AF demagnetization behavior, as well as high fidelity samples 76535 (Garrick-Bethell et al., 2009) and 10020 (Shea et al., 2012). We show that the unstable demagnetization behaviors observed for 15556, 15016, and 12017 likely result from the combined effects of multidomain magnetic carriers, magnetic anisotropy, and spurious ARM. We conclude that while the unstable demagnetization data for 15556, 15016, and 12017 clearly do not provide evidence for the presence of a lunar dynamo at 3.2–3.4 Ga, they also do not require the absence of a dynamo-generated magnetic field on the Moon at this time.

2. Description of analyzed lunar samples

2.1. Petrologic descriptions

15556 is a fine-grained, highly vesicular, olivine-normative basalt (Meyer, 2008) with an $^{40}Ar/^{39}Ar$ age of ~3.4 Ga (Kirsten et al., 1972). Our petrographic analyses (see Supplementary material) found no evidence of shock, implying peak shock pressures < 5 GPa: plagioclase crystals do not show any mechanical twinning, fracturing, or alteration to maskelynite, and there is no undulatory extinction in olivine (Fig. S3a). Thermomagnetic curves identified kamacite ($Fe_{0.94-0.96}Ni_{0.04-0.06}$) as the main ferromagnetic constituent in 15556 (Nagata et al., 1972, 1973). Our elemental abundance analyses of metal grains using a JEOL-JXA-8200 electron microprobe at the Massachusetts Institute of Technology found that kamacite occurs as isolated 2–30 μm diameter blebs ($Fe_{0.94}Ni_{0.06}$) as well as ~5 μm diameter grains of nearly pure iron intergrown with troilite (Table S2).

15016 is a medium-grained, highly vesicular, olivine-normative basalt (Meyer, 2008) with Rb/Sr and $^{40}Ar/^{39}Ar$ ages of 3.3–3.4 Ga (Evensen et al., 1973; Kirsten et al., 1972). 15016 does not show any petrographic evidence of shock (peak shock pressure < 5 GPa) (Fig. S3b). Our microprobe analyses identified 2–3 μm diameter metallic iron associated with troilite as well as 10 μm diameter free kamacite ($Fe_{0.87-0.93}Ni_{0.07-0.13}$) (Table S2).

12017 is a medium-grained pigeonite basalt (Meyer, 2008; Warner, 1970) lacking shock features (Fig. S3c) with an $^{40}Ar/^{39}Ar$ age of 3.2 Ga (Horn et al., 1975). The basalt is coated on one side with an impact glass estimated to be ~4–20 thousand years (ky) old (Fleischer et al., 1971; Morrison et al., 1973) (Table S2). The subsamples used in our paleomagnetic experiments were taken from both basaltic (12a2, 12a1c, and 13b1) and glass (12b, 13a2, and 59) lithologies. In the basalt portion, our microprobe analysis identified 3–5 μm metallic iron blebs in troilite as well as 50 μm free metal grains with composition $Fe_{0.99}Ni_{0.01}$. The glass portion contained 20 μm blebs of iron phosphide with ≤1 μm iron sulfide inclusions. Furthermore, ≤1 μm blebs of kamacite were distributed throughout the glass (Table S2). The latter grains were too small for accurate quantitative elemental analyses.

10020 is an apparently unshocked (peak shock pressure < 5 GPa) (Fig. S1d), fine-grained low-K ilmenite basalt (Kramer et al., 1977; Meyer, 2008) with an $^{40}Ar/^{39}Ar$ age of 3.72 Ga (Geiss et al., 1977; Guggisberg et al., 1979; Shea et al., 2012). Our microprobe analysis identified 0.1–5 μm metallic iron (negligible Ni content) blebs in troilite (Table S2).

76535 is an apparently unshocked (peak shock pressure < 5 GPa), coarse-grained troctolite (Meyer, 2008) dated to 4.2 Ga using a variety of chronometers [see Garrick-Bethell et al. (2009)]. The sample contains kamacite and taenite as free blebs and as inclusions in plagioclase [see Garrick-Bethell et al. (2009)].

2.2. Domain state

We assessed the domain state of samples 15556, 15016, 12017, and 10020 by measuring hysteresis loops and first order reversal curves [FORCs; see Pike et al. (1999)] (see Supplementary material). Ratios of saturation remanent magnetization (M_{rs}) to saturation magnetization (M_s) and remanent coercivity (H_{cr}) to coercivity (H_c) (Dunlop, 2002a, b) and FORC distributions indicate that all four samples are predominantly multidomain (Figs. S4 and S5 and Table S3), consistent with previous studies (Cournede et al., 2012; Gattacceca et al., 2010; Nagata et al., 1972, 1973; Pearce et al., 1973; Shea et al., 2012). Previous hysteresis studies also indicated a dominantly multidomain grain size for 76535 (Garrick-Bethell et al., 2009) (Table S3). While 10020 and 76535 have an average grain size in the multidomain range, their hysteresis parameters (higher M_{rs}/M_s, lower H_{cr}/H_c) suggest that they are less coarse-grained than samples with poor NRM demagnetization behavior (15556, 15016, and the 12017 basalt; see Sections 3.2–3.4) (Fig. 2). This relationship is confirmed by our FORC analyses, which indicate that 10020 has an additional population of higher coercivity grains relative to 15556, 15016, and the 12017 basalt (Fig. S5) as well as our coercivity spectra (see below).

2.3. Rock magnetic studies

We conducted a variety of rock magnetic experiments on 15556, 15016, 12017, and 10020 to characterize magnetostatic interactions, their coercivity spectra, and their median destructive fields (MDFs) (see Supplementary material). Paleomagnetic and rock magnetic remanence experiments were conducted using a 2G Enterprises Superconducting Rock Magnetometer 755 equipped with automated sample handling and demagnetization equipment (Kirschvink et al., 2008) in a magnetically shielded room (field < 200 nT) housed in the MIT Paleomagnetism Laboratory (http://web.mit.edu/paleomag). The magnetometer has a sensitivity of to $\sim 1 \times 10^{-12}$ Am^2, at least 2 orders of magnitude lower than nearly all magnetic moments measured here. Four

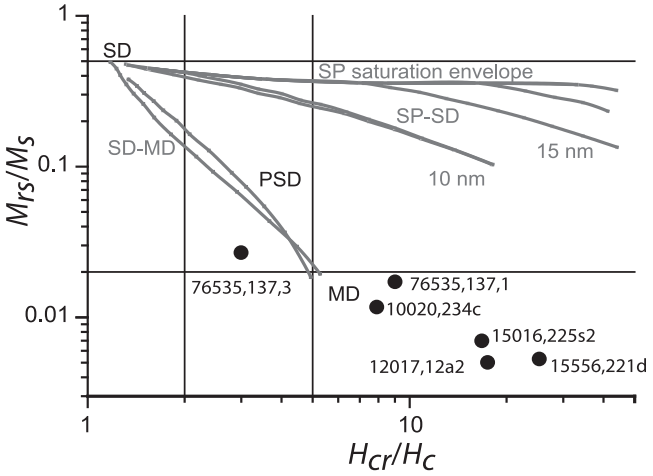

Fig. 2. Dunlop–Day plot of hysteresis parameters. The ordinate gives the magnitude of the saturation remanent magnetization (M_{rs}) divided by the magnitude of the saturation magnetization (M_s). The abscissa gives the remanent coercivity (H_{cr}) divided by the coercive force (H_c). Black circles designate sample positions. Straight black vertical and horizontal lines divide the plot into rectangular regions representing single domain (SD), pseudo-single domain (PSD), and multidomain (MD regimes. Note that this plot was developed for magnetite-bearing samples and should only be used for a qualitative understanding of grain size trends for the kamacite-bearing samples shown here.

readings of magnetic moment were made and averaged for each measurement, and circular standard deviations were typically $<2^{\circ}$. Samples which exhibit spurious AF demagnetization (15556, 15016, and basalt 12017; see Supplementary material) display lower remanent coercivities and median destructive fields for ARM and isothermal remanent magnetization (IRM) than 10020 and the 12017 glass, which have stable demagnetization patterns (Supplementary material, Table S4 and Fig. S6). These results are consistent with the hysteresis properties (Section 2.2), which suggest that low magnetic fidelity samples (i.e. 15556, 15016, and the 12017 basalt) contain a larger fraction of multidomain magnetic carriers than high fidelity samples 10020 and the 12017 glass (see Section 4.3).

The low remanent coercivities and MDFs of samples 15016 and the 12017 basalt mean that their putative primary TRM (if present) may have been partly demagnetized by shock during impact excavation, because shock pressures of just 2 GPa can demagnetize grains with coercivities up to $\sim$30 mT (Gattacceca et al., 2008). On the other hand, higher coercivity samples like 10020 and the 12017 glass should still be able to retain some primary TRM (if present), even if they have experienced some shock effects.

3. Natural remanent magnetization

3.1. Methodology

We studied the NRM behavior of mutually oriented subsamples of 15556, 15016, 12017 (basalt and glass portions), and 10020. We used AF rather than thermal demagnetization because the former should more efficiently remove secondary IRM and SRM overprints which are blocked by coercivity rather than blocking temperature. Such overprints have been ubiquitously observed in lunar samples. Thermal demagnetization associated with the Thellier–Thellier paleointensity method is also disadvantageous because it typically causes alteration of the metallic magnetization carriers in lunar rocks.

All subsamples except those from 12017 were taken from the non-space-weathered interiors of their parent rocks. The samples were subjected to identical progressive three axis AF demagnetization sequences up to 85 mT, with some subsamples further demagnetized up to 290 mT. Antiparallel treatment orientations were not used due to sample mounting restrictions. We measured the magnetic moment after AF application in each of the three orthogonal (N, E, Z coordinate) directions and computed the final moments as the average of all measurements for each AF level [after Garrick-Bethell et al. (2009)] in order to reduce spurious ARM and GRM (see Section 1).

We used principal component analysis (PCA) (Kirschvink, 1980) to determine the best-fit directions for the magnetization components in each sample and the dANG/MAD test to qualitatively assess whether a magnetization component trends toward the origin [see Lawrence et al. (2008)]. This method compares the angular difference between a non-origin-constrained least squares fit of the NRM component and the centroid of the least squares fit (dANG) to the maximum angle of deviation (MAD) of the fit. Although this test is somewhat arbitrary because it does not assign a confidence interval to the hypothesis that the NRM component is origin-trending, we adopt it here in the absence of more robust statistical tests (see Supplementary material).

We tested for GRM acquisition in our samples following Garrick-Bethell et al. (2009) (see Section 3.2 of their Supplementary Online Material). We found that GRM does not significantly contribute to the demagnetization behavior of our mare basalts (see Supplementary material and Fig. S7).

3.2. Summary of demagnetization results

All subsamples from 15556, 15016, and 12017 analyzed in this study exhibited unstable behavior during demagnetization of NRM (Fig. 3). Repeated AF steps at a single field level led to large changes in moment. This variability is certainly unrelated to the moment sensitivity of our magnetometer because repeat measurements (without intervening demagnetization) were essentially identical and the measured moments were at least two orders of magnitude above our instrument's detection limit. Furthermore, the magnetic fields inside our shielded room and AF coils are <200 nT so the cause of unstable demagnetization cannot be induced moments or ARM acquired in a time-varying background field. Rather, as described below, the unstable AF behavior observed in our samples appears to be the product of spurious ARM and remanence anisotropy.

Low coercivity (LC) magnetization components blocked from to $\sim$10 mT could be identified in 15 out of 17 subsamples. Only 4 out of 17 subsamples clearly had additional higher coercivity (HC) components, and even these were only blocked to low coercivities (<25 mT) (see Supplementary material, Table S5). For sample 15556, which had three subsamples with clear HC components, both the LC and HC components of these subsamples were generally non-unidirectional with respect to each other (Fig. S8). One subsample, 15556,221c displayed a spectacular case of magnetic pinning where the moment flipped repeatedly between two antipodal directions during AF application up to 290 mT (see Fig. 3b and S9). For subsamples lacking easily identifiable HC components (the vast majority of subsamples), we fit nominal HC components in order to later demonstrate that this AF range yields paleointensity ranges with high uncertainties that make them indistinguishable from zero (null field) (see Section 4.2). Given this behavior, our NRM data for 15556, 15016, and 12017 clearly do not provide any evidence for the existence of an ancient lunar dynamo when these samples formed between 3.2 and 3.4 Ga.

4. Paleointensity studies

4.1. Introduction

A major goal of lunar paleomagnetism studies is to determine the paleointensity of the ancient magnetizing field. For the reasons described in Section 3.1, we chose to use the nondestructive, AF-based ARM and IRM methods to estimate absolute paleointensities for the HC components of our samples (see Supplementary material). These methods are similar to those used for paleointensity studies during the Apollo era, allowing us to assess the meaning of these previous results in the context of the magnetic recording fidelity of the rocks.

4.2. NRM paleointensity results

Paleointensity results for sample 10020 provide robust evidence for Earth-strength fields on the Moon (Shea et al., 2012). However, most paleointensity experiments on 15556, 15016, and 12017 were inconclusive (see Supplementary material). Most subsamples either yielded formally negative (i.e., meaningless) paleointensities or had formal uncertainties exceeding their corresponding paleointensity values (Table S7) indicating that they are consistent with zero magnetizing field. These results, coupled with the noisy NRM demagnetization behavior observed for these samples, led us to examine their magnetic recording fidelity. Our goal was to determine whether certain samples are intrinsically incapable of stable AF demagnetization behaviors.

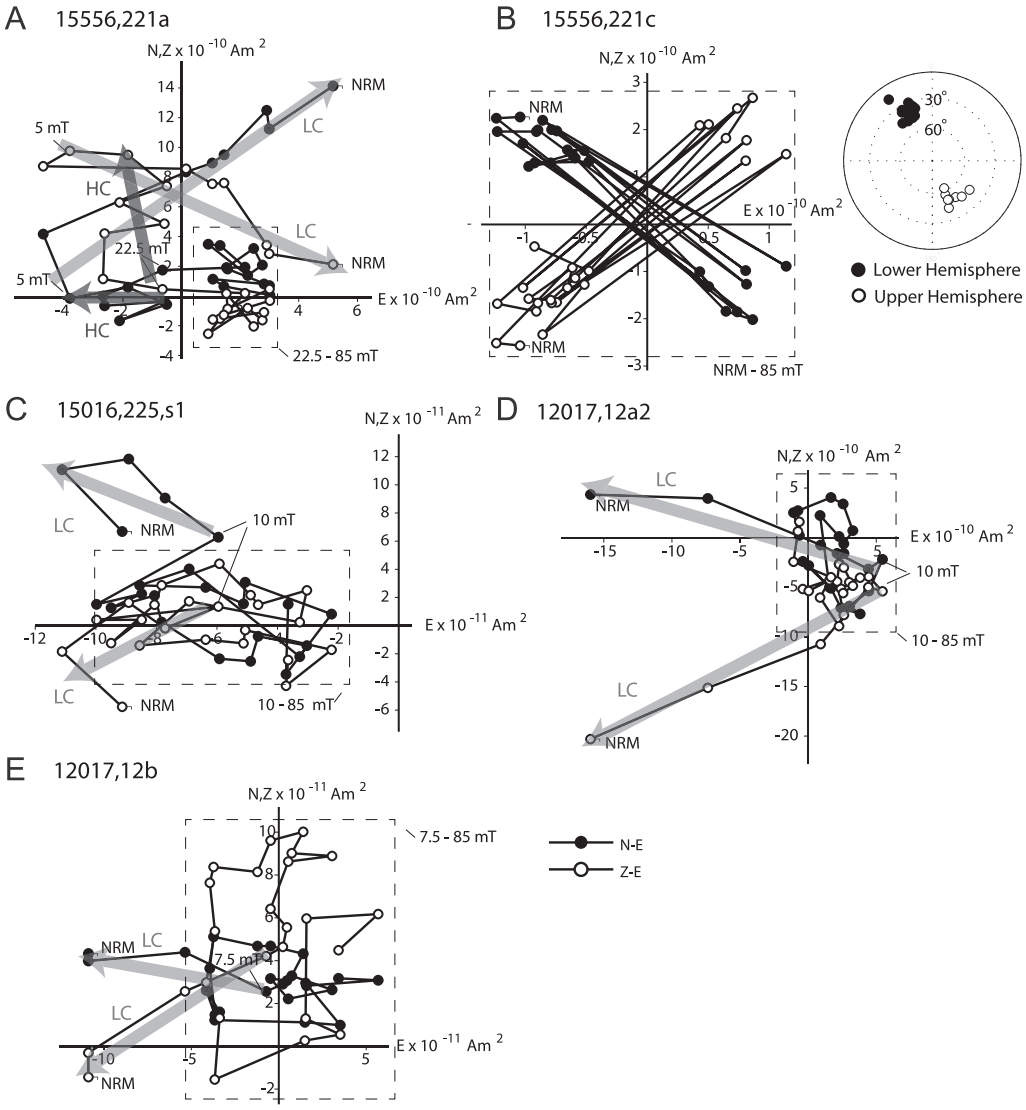

Fig. 3. NRM demagnetization data for lunar samples. Shown for each sample are two-dimensional projections of the NRM vector during AF demagnetization. Closed symbols represent end points of magnetization projected onto the horizontal (N and E) plane. Open symbols represent end points of magnetization projected onto the vertical (Z and E) plane. Peak fields for selected AF steps are labeled in mT. Low coercivity (LC) and high coercivity (HC) magnetization components are labeled and represented with light gray and dark gray arrows, respectively. (A) 15556,221a. (B) 15556,221c. Inset shows equal-area stereographic presentation of data. Data shown for this subsample have been downsampled to every fifth AF step and were not averaged using the Zijderveld–Dunlop method. For full demagnetization data see Fig. S7. (C) 15016,225s1. (D) basalt 12017,12a2. (E) glass sample 12017,12b.

If a sample has low magnetic recording fidelity, it cannot be used to determine whether a paleomagnetic field was present on its parent body.

4.3. Paleointensity limit tests

We conducted the following experiment to assess the magnetic recording fidelity of our samples. At least one subsample from each parent rock was imparted with a laboratory ARM using DC bias fields ranging from 3 μT to 200 μT and an AC field of 85 mT to simulate TRM acquisition at paleofields ranging from 2–150 μT [using an TRM/ARM ratio of 1.34 measured for some lunar rocks; see Stephenson and Collinson (1974)]. We then used the ARM method to retrieve paleointensities for each applied lab field. A comparison of retrieved paleointensities against the applied (known) intensity that produced the laboratory remanence indicates the magnetic recording fidelity of a sample. This approach is analogous to a TRM experiment previously used for ordinary chondrites (Brecher and Leung, 1979). The closer a retrieved paleointensity value is to the applied lab field intensity and its estimated uncertainty due to unstable AF behavior, the more likely a magnetization can be successfully retrieved using AF methods. We quantified this agreement as a function of applied field strength using two metrics that we call difference (D) and error (E):

$$D \equiv |L-I|/L \cdot 100\% \quad (1)$$

$$E \equiv W/L \cdot 100\% \quad (2)$$

The first metric quantifies the difference between the TRM-equivalent value of the applied laboratory field (L) and the retrieved paleointensity (I) (Fig. 4a). The second metric quantifies the error associated with the paleointensity measurement by comparing the width of the Student's t-test-derived 95% confidence interval (W) for the retrieved paleointensity to the magnitude of the applied laboratory field (see Supplementary material) (Fig. 4b). We used two metrics because it is possible for a retrieved paleointensity to be close in value to the applied

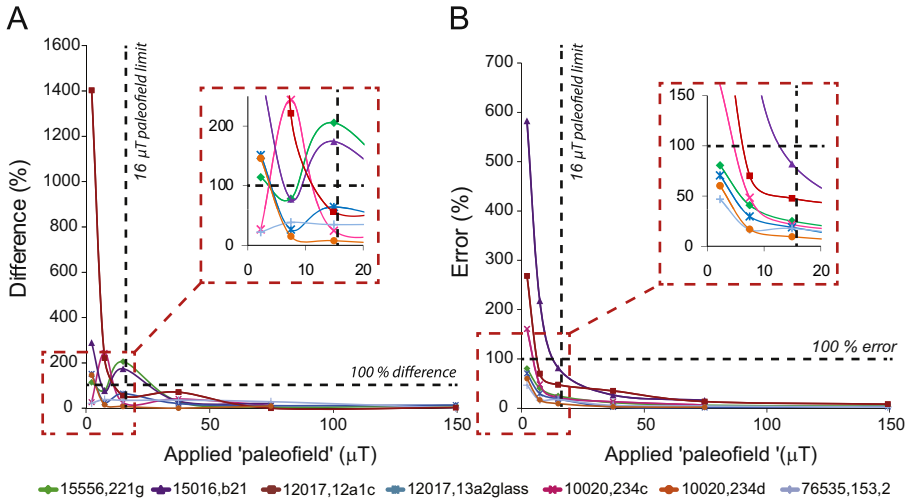

Fig. 4. Artificial paleointensity tests on lunar samples. (A) Difference and (B) error for retrieved paleointensities versus magnitude of applied laboratory field for samples 15556,221g (green diamonds), 15016,b21 (violet triangles), 12017,12a1c (maroon squares), 12017,13a2 (teal stars) 10020,234c (pink crosses), 10020,234d (orange circles), and 76535,153,2 (light blue pluses). See Section 4.3 for definitions. In (A), the dashed horizontal line denotes the threshold of 100% difference between the applied field and the retrieved paleointensity. In (B), the dashed horizontal marks the threshold where the width of the 95% confidence interval of the retrieved paleointensity is equal in magnitude to the applied laboratory field. Shown in both parts (A) and (B) is the 16 μT estimated maximum surface paleointensity limit for a dynamo generated by a 375 km radius lunar core in magnetostrophic balance (Wieczorek et al., 2006).

laboratory field (i.e., have a low value for D), but for the formal error associated with the experiment due to nonideal demagnetization behavior to be larger than the magnitude of the paleointensity (i.e., have a large value for E). Both metrics should have low values for a paleointensity to be considered high quality. Here we define a sample to be a good magnetic recorder at those field strengths for which the following conditions are satisfied: (a) there is less than 100% difference between the applied field and retrieved paleointensity and (b) there is less than 100% error associated with the measurement. These thresholds are somewhat arbitrary but are certainly generous towards poor recorders: it is virtually certain that samples that do not meet these thresholds are nonideal for paleointensity studies.

We found that AF demagnetization of magnetization produced in higher applied lab fields exhibited more ideal behavior than magnetization produced with weak fields (Fig. S10). Weak-field magnetizations were prone to spurious demagnetization, which in turn resulted in less accurate retrieved paleointensities during the experiment described in the preceding paragraph. We found that AF methods can retrieve TRM-equivalent fields down to 7 μT for 10020,234d and glass 12017,13a2, and as weak as 2 μT for 76535,153. By comparison, we could only retrieve TRM-equivalent fields down to 37 μT for basalts 15016,b21 and 15556,221g. Furthermore, heterogeneities in magnetic recording fidelity may exist within a single sample. For example, we found that we could retrieve TRM-equivalent paleointensities as weak as 7 μT from 10020,234d but only down to 15 μT for 10020,234c. This difference in recording fidelity is mirrored by observed differences in NRM demagnetization behavior between these two subsamples [compare Shea et al. (2012)'s Fig. S3A,C with their Fig. S3B]. Therefore, a computed paleointensity from a subsample should ideally only be compared with the field recording limit determined for the same subsample when assessing the reliability of paleointensity estimates. In summary, only high-fidelity samples such as 10020, 76535, or the 12017 glass are capable of stable AF demagnetization and providing reliable AF-based paleointensity values from the predicted weak fields (<16 μT) from a lunar dynamo. Paleointensities from intermediate fidelity samples should be scrutinized subsample-by-subsample. AF-based paleointensity results from poor magnetic recorders (e.g., 15016, 12017 basalt, and 15556) should be regarded with caution.

4.4. Implications for Apollo-era paleointensity methods

We have shown that nonideal AF demagnetization and inaccurate paleointensity determinations may be caused by spurious ARM. This conclusion led us to re-assess previous lunar paleointensity analyses conducted using AF-based techniques. The majority of IRM paleointensities acquired during the Apollo era used the $NRM_{20}/sIRM_{20}$ normalization method [termed the "REMc" method by Acton et al. (2007)] in which NRM AF demagnetized to 20 mT (TRM_{20}) was compared to sIRM AF demagnetized to 20 mT ($sIRM_{20}$) (Cisowski et al., 1983; Fuller and Cisowski, 1987). This method was used because many samples exhibited low-field (<10 mT) IRM overprints that would otherwise contaminate paleointensities derived from ratios of undemagnetized NRM and IRM. A major problem with this method is that highly multidomain lunar samples and synthetic samples displayed a non-linear relationship between laboratory TRM_{20} to $sIRM_{20}$ when the TRM was applied in weak fields (<10 μT) (Cisowski et al., 1983; Fuller and Cisowski, 1987). The reason for this behavior was left unexplained and led the authors to question the fidelity of the majority of Apollo-era paleointensity values.

Our results described above suggest this nonlinear behavior may be a manifestation of ARM noise. To test this hypothesis, we studied the relationship between laboratory ARM which was AF demagnetized to 20 mT (ARM_{20}) and $sIRM_{20}$ on the same subsamples used in the preceding section (see Supplementary material for further discussion of our methodology and results). We observed a nonlinear relationship between ARM_{20} and $sIRM_{20}$ at ARM DC fields ranging from 3–200 μT (equivalent to TRM acquired at 2–150 μT) (Fig. 5a). For comparison, we examined the relationship between total ARM and total sIRM (i.e., that were not subsequently demagnetized) (ARM_0 and $sIRM_0$). In this case, we observed a linear relationship between ARM_0 and $sIRM_0$ (analogous to non-demagnetized TRM and sIRM) for almost all samples down to their recording limits (Fig. 5b). Given that we have shown that highly multidomain samples are extremely

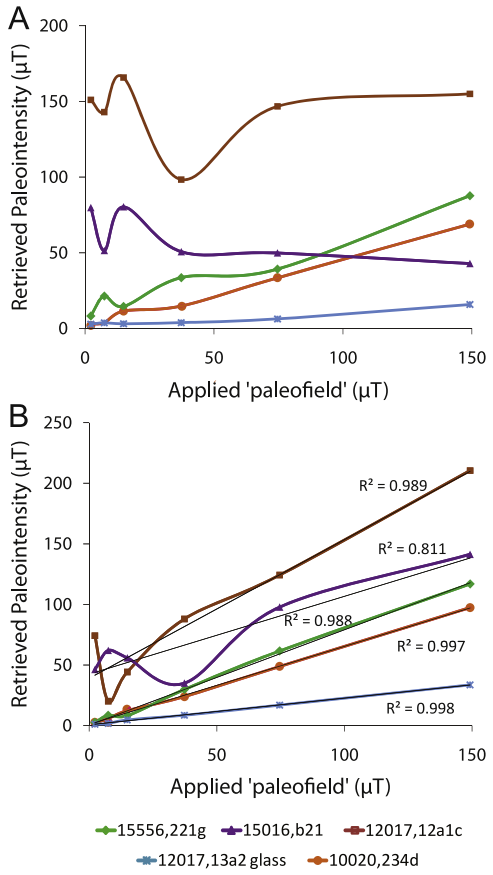

Fig. 5. Simulated paleointensity tests using the (A) $ARM_{20}/sIRM_{20}$ normalization method, (B) total ARM/sIRM (i.e., without AF demagnetization). Plots show retrieved paleointensities versus applied laboratory fields. Featured samples are: 15556,221g (green diamonds), 15016,b21 (violet triangles), 12017,12a1c (maroon squares), 12017,13a2 (teal stars), and 10020,234d (orange circles).

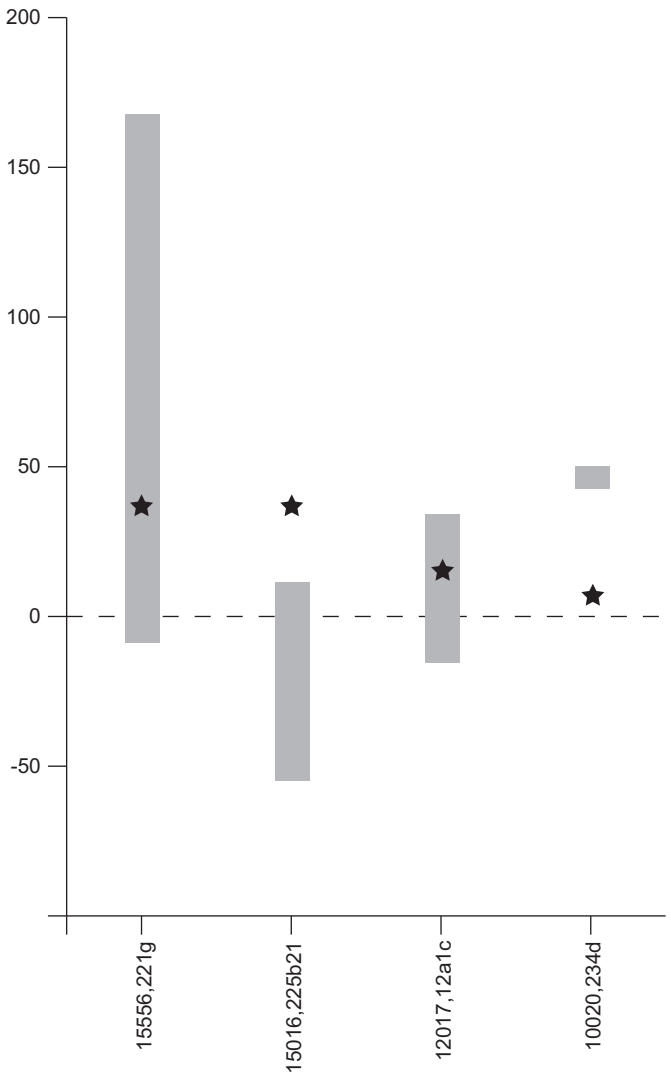

Fig. 6. Calculated paleointensities and paleofield recording limits measured for various lunar samples. Gray rectangles show the paleointensities (including formal uncertainties) computed for AF ranges of 23–85 mT for each sample (name listed along bottom axis) using the ARM and IRM methods. This range of AF fields was used to calculate paleointensities for this plot in order to avoid inclusion of possible low-coercivity overprints on samples. Paleointensity values reported for 10020 are from Shea et al. (2012). Black stars show the minimum paleofield required to retrieve accurate paleointensities using the ARM method.

susceptible to spurious ARM, we propose that the nonlinear relationship between ARM_{20} and IRM_{20} and between TRM_{20} and $sIRM_{20}$ observed by Cisowski et al., 1983, Fuller and Cisowski (1987) and in our Fig. 5a is a manifestation of ARM noise introduced by the AF application used in these experiments. Unfortunately, this problem cannot be reconciled by simply computing ratios of undemagnetized NRM and sIRM due to the ubiquitous presence of low coercivity overprints (typically secondary IRM) in lunar samples.

A related longstanding unsolved issue in lunar paleointensity studies observed specifically when using the REMc paleointensity method is that there appears to be a minimum paleofield ($NRM_{20}/sIRM_{20} \geq 3.6 \times 10^{-4}$, implying paleointensities $\geq 1\,\mu T$) that has been retrieved, regardless of sample age (Cisowski et al., 1983). This minimum field, which is far stronger than nearly all putative field sources other than a core dynamo, is even observed in samples < 1.5 Ga in age when a dynamo is highly unlikely due to a lack of power sources [see Dwyer et al., 2011; Le Bars et al., 2011; Stegman et al., 2003]. Our results indicate that all AF-based paleointensity experiments will give highly inaccurate values if the field that magnetized the samples has a lower intensity than the minimum limit that can be retrieved due to ARM noise (Fig. 6). Specifically, when using the REMc normalization method, spurious ARM may inflate values for ARM_{20}, yielding high ($\geq 1\,\mu T$) paleointensities for samples which may have nevertheless formed in a zero-field environment after the end of a lunar dynamo. This suggests that REMc paleointensity values measured for young samples with ages of several hundred Ma may only be upper limits and should be reevaluated using more robust paleointensity techniques.

5. Zig-zag behavior

We have discussed the observation of unstable AF demagnetization behavior present during demagnetization of both NRM and induced ARM (as a proxy for TRM) in some lunar samples. Magnetic anisotropy studies on these samples may shed light on sources of the more ordered spurious behaviors that have been observed, like zig-zag demagnetization and pinning of magnetization directions. We next discuss how magnetic anisotropy in combination with spurious ARM may responsible for these behaviors.

The flipping of the magnetic moment of sample 15556,221c between two nearly antipodal directions suggests that magnetic anisotropy is the source for zig-zag demagnetization. This is

because anisotropy preferentially constrains magnetization to easy axes and planes. We conducted ARM and IRM anisotropy of remanence experiments on various subsamples of basalts 15556, 15016, 12017, and 10020 (Tables S8 and S9). We applied ARM (DC field of 2 mT and AC field of 800 or 850 mT) and IRM (20 mT field) along all three orthogonal axes and solved for the principal axes of the anisotropy ellipsoids [following Stephenson et al. (1986)]. We averaged the results of each experiment (two ARM and two IRM experiments) for all samples except the 12017 glass (which only had one ARM experiment and one IRM experiment) to reduce uncertainties associated with sample orientation ($\pm 5^{\circ}$). The nature of the anisotropy of remanence in each sample can be characterized by two parameters: the degree of anisotropy, *P*, and the shape factor, *T*. *P* is defined as the ratio of the magnetic moments acquired along the easy axis and hard axes of the anisotropy ellipsoid. *T* is calculated from relative ratios of moments acquired along the easy, medium, and hard axes, and provides information regarding the shape of the anisotropy ellipsoid. Positive values of *T* indicate oblate ellipsoids, while negative values indicate prolate ellipsoids.

We found that sample 15556,221c, which exhibited zig-zag demagnetization, is by far our most strongly anisotropic sample and has an oblate fabric ($P=2.0$, $T=0.17$ for ARM; $P=2.6$, $T=0.30$ for IRM) and a well-defined easy plane (i.e., plane defined by the easy and intermediate magnetic axes). The two antipodal pinned directions lie within 22.5° from the easy axis of magnetization and within 18° of the easy plane (Fig. 7). We estimate that the uncertainty of this easy plane orientation to be $<3^{\circ}$, based on the differences in the location of the pole of the easy plane (hard axis direction) between experiments. The MAD values derived from PCA fits for each of the two directional groups are 27.7° and 31.6°. Since the angular distances between the pinned magnetization directions and the easy plane are less than the MADs of the PCA fits, the magnetization directions essentially fall within error of the easy plane. This demonstrates that pinning during AF demagnetization is very likely due to the high magnetic anisotropy of this subsample. Similar but preliminary observations using susceptibility anisotropy were reported for several lunar samples with spurious remanence by Brecher (1977).

Anisotropy alone cannot explain why the moment of 15556,221c flips back and forth in the easy plane as opposed to being stably oriented in one direction. As discussed above (Sections 3 and 4), 15556 is highly susceptible to acquisition of spurious ARM during AF demagnetization. We propose that spurious ARM is also responsible for the flipping observed for 15556,221c. To test this hypothesis, we repeated AF applications multiple times for each applied field level during demagnetization of NRM (as described in Section 3.1). We counted how many times the magnetic moment flipped between antipodal directions for each AF level and determined the fraction of AF applications which led to flips. In general, the flipping frequency increased with AF level up to 10 mT before leveling off at a 50% chance of flipping at any given AF application (see Supplementary material and Fig. S12). This increase suggests that ARM noise is the causative factor because the net moment becomes increasingly dominated by spurious ARM at progressively higher AF steps. If flipping was solely controlled by an unbiased AC field with random thermal fluctuations, one would expect the 50% flipping frequency to start at the first flip at the AF level of the first flip (3 mT). This likely explains similar pinning and zig-zag demagnetization observed in other lunar samples (Brecher, 1976; Hoffman and Banerjee, 1975).

We found that the other subsamples of 15556 were less anisotropic than 15556,221c, with *P* values ranging from 1.13–1.52. Subsamples of 12017 and 15016 had similar values with average $P=1.14$ and 1.55, respectively (Tables S8 and S9). 10020,234b4 and 10020,234d had average *P* ranging from 1.12–1.73, respectively [see Shea et al. (2012)]. Our anisotropy results, in conjunction with other remanence anisotropy parameters previously published for lunar rocks by Cournede et al. (2012) and Potter (2011), indicate an inverse correlation between *P* and sample size (Fig. 8). This likely indicates that the anisotropy is a

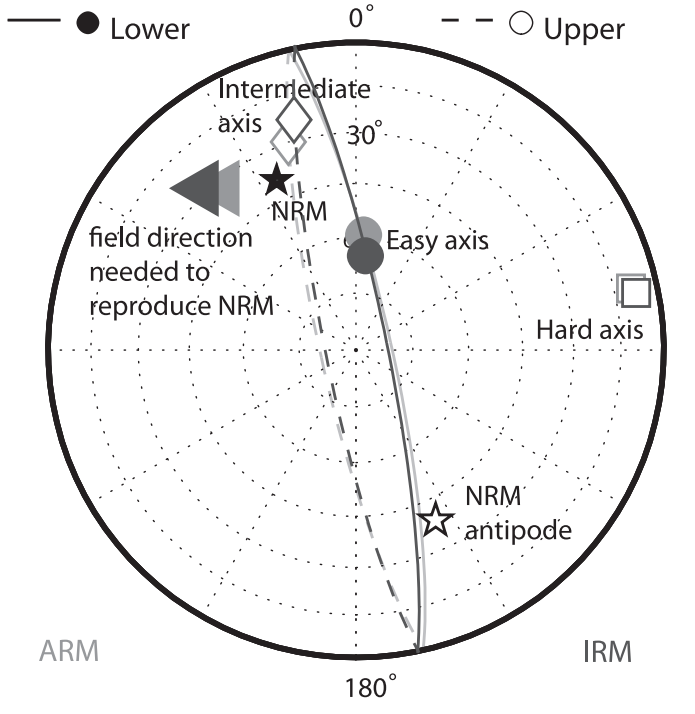

Fig. 7. Equal area stereographic projection of anisotropy of remanence results for sample 15556,221c. Open symbols and dashed lines represent points and portions of great circles in the upper hemisphere. Closed symbols and solid lines represent points and portions of great circles in the lower hemisphere. Stars represent the NRM direction and its antipode. Circles, diamonds, and squares represent the easy, medium, and hard directions of the remanence anisotropy ellipsoids, respectively. Light gray symbols represent results from the ARM experiment, while dark gray symbols represent those from the IRM experiment.

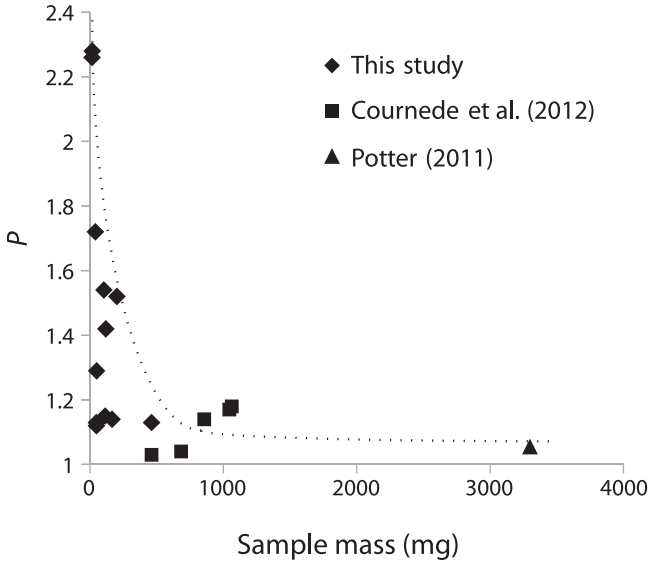

Fig. 8. Degree of anisotropy (*P*) vs. mass of all samples subjected to anisotropy of remanence experiments in this study. Dashed line highlights trend in data. Anisotropy results from this study are represented by diamonds, while those from Cournede et al. (2012) and Potter (2011) are represented by squares and triangles, respectively.

reflection of a small number of metal grains with shape anisotropy which are likely to dominate samples with small masses.

6. Discussion

The unbrecciated, unshocked, primary igneous textures of basalts 15556, 15016, and 12017 would at first glance appear to make them ideal candidates for lunar paleomagnetism studies. However, like many other lunar samples reported in the literature (Table S1), these samples behave unstably during AF demagnetization experiments and are poor recorders of magnetic fields of strengths predicted for an ancient lunar dynamo. Their NRM does not decline monotonically toward the origin with application of increasing peak AF fields. There is a large amount of scatter in both magnitude and direction of remanent magnetization at AF fields above 20 mT. This is a clear demonstration of the deleterious effects of spurious ARM acquired during AF demagnetization. As discussed in the Supplementary material, scatter in moment magnitude and direction resulting from acquisition of spurious ARM may cause noisy HC magnetization directions to appear origin-trending (i.e. primary) in the dANG/MAD test when they may or may not actually be. Alternatively, ARM noise may obscure an otherwise origin-trending magnetization, further complicating the task of determining whether the magnetizations of low-fidelity lunar samples can be primary TRM. One subsample, 15556,221c, exhibited anisotropy-controlled pinning behavior, with the magnetization direction flipping between two antipodal directions without decaying in intensity. None of our basalt samples acquired significant GRM, although it has previously been shown that GRM significantly affects 76535 (Garrick-Bethell et al., 2009).

Our hysteresis and rock magnetic studies show that mare basalts 15556, 15016, and 12017 possess a higher fraction of multidomain kamacite than samples which express stable AF demagnetization such as 10020, the 12017 glass, and 76535. As explained in Section 1, samples dominated by multidomain magnetic carriers possess lower coercivities and are more susceptible to spurious ARM noise. This explains why some subsamples are almost completely demagnetized at low AF amplitudes (below 20 mT). The greater susceptibility to GRM acquisition of 76535 likely relates to the relative finer grain size of its ferromagnetic minerals relative to the other samples in this study.

Spurious ARM noise also affects IRM and ARM paleointensity studies, which rely on AF demagnetization as part of the paleointensity method. This effect means that most samples with unstable AF demagnetization will not provide accurate AF-based paleointensities for paleofields weaker than a certain threshold value. We observe a threshold of $\sim$37 μT for two of the basalt subsamples analyzed during this study. This value is above the theoretical estimates of the maximum lunar surface field that could be generated by a small lunar core Dwyer et al., 2011; Le Bars et al., (2011); Wieczorek et al., 2006). Therefore, many lunar rocks are not suitable for AF-based paleointensity studies of expected lunar field intensities. This conclusion has major implications for our current understanding of the lifetime of the lunar dynamo that has been inferred from REMc paleointensities. In particular, spurious ARM may be also be responsible for the minimum $\sim$1 μT paleofield consistently estimated for samples younger than the expected lifetime of an ancient lunar dynamo [see Fig. 3.22 of Wieczorek et al. (2006)].

For samples susceptible to spurious ARM, better demagnetization and paleointensity techniques are necessary. If thermal demagnetization and Thellier–Thellier techniques can be developed so as to avoid alteration, they could be powerful tools for understanding the true nature of lunar remanent magnetization. Experiments on terrestrial rocks have successfully retrieved paleofields as low as 1 μT (Tanaka and Kono, 1984). These results demonstrate that thermal-based techniques are in principle capable of recovering the weak ($<$15–20 μT) fields expected for the lunar dynamo. Using the Thellier–Thellier technique, Lawrence et al. (2008) were able to successfully recover paleointensities of just 5 μT from laboratory TRMs for three lunar samples, two of which were demonstrably multidomain (Lawrence and Johnson, 2009) (with the important caveat that at least two of these samples had been altered during previous thermal demagnetization experiments). However, even if thermal methods could be perfected to entirely avoid alteration, AF methods may still be required to remove low coercivity overprints. Therefore, the development of low-ARM noise AF systems may be a preferable alternative for future lunar paleomagnetic studies.

As described in Section 5, we observed a correlation between sample size and degree of anisotropy *P*. A similar correlation was previously observed in anisotropy of magnetic susceptibility (AMS) studies on the Knyahinya L/LL5 chondrite by Gattacceca et al. (2005). Larger samples have the advantage of having more ferromagnetic grains that contribute to the magnetization, which tempers the effects of magnetic anisotropy from individual grains. Therefore, it may be beneficial to conduct paleomagnetic analyses on larger subsamples. Our experiments on lunar basalts (Fig. 8) suggest that a minimum sample size for mare basalts should be $\sim$150 mg.

7. Conclusions

- Unstable AF demagnetization behavior, observed in some lunar samples as well as meteorites, often makes it difficult to determine whether ancient magnetic fields existed on their parent bodies.
- Multidomain samples often have poor demagnetization behavior and yield unreliable absolute paleointensities using AF-based methods. This is a particular problem for extraterrestrial paleomagnetism because of the predominance of multidomain carriers and the more widespread use of AF demagnetization relative to Earth paleomagnetism.
- Spurious ARM noise and magnetic anisotropy can explain unstable AF demagnetization and pinning in extraterrestrial samples.
- GRM acquisition is likely a problem of secondary importance since it was only observed in one of the samples considered here. This is likely due to the dominant multidomain grain sizes of the samples.
- Better techniques need to be developed to study samples susceptible to spurious ARM. Possibilities include low-noise AF systems and thermal demagnetization and Thellier–Thellier methods that avoid sample alteration.
- Spurious ARM may be responsible for $\geq$1 μT paleointensities previously computed for samples likely to postdate a lunar dynamo.
- Unless a sample can be shown to preserve stable low-field laboratory induced TRM or ARM, unstable AF demagnetization of does not provide evidence against the presence of an ancient lunar dynamo.

Acknowledgments

We thank CAPTEM for allocating the samples and the staff of the NASA Lunar Sample Laboratory for assistance in sample preparation and acquisition. We also thank F. Demory of CEREGE

and J. Bowles at the Institute of Rock Magnetism for assistance in acquiring hysteresis and FORC measurements, N. Chatterjee for assisting with microprobe measurements, R. Fu with developing methods for accurate low bias field ARM acquisition, and C. Ross for use of her vibrating sample magnetometer. SMT and EKS were supported by a NASA Earth and Space Science Fellowship. SMT was supported by a National Science Foundation Graduate Research Fellowship and the NASA Lunar Science Institute. This work was also supported by grants from the NASA Lunar Advanced Science and Exploration Research Programs to BPW and the NASA Lunar Science Institute to BPW and TLG.

Appendix A. Supporting information

Supplementary data associated with this article can be found in the online version at http://dx.doi.org/10.1016/j.epsl.2012.05.024.

References

Acton, G., Yin, Q.Z., Verosub, K.L., Jovane, L., Roth, A., Jacobsen, B., Ebel, D.S., 2007. Micromagnetic coercivity distributions and interactions in chondrules with implications for paleointensities of the early solar system. J. Geophys. Res., 112, http://dx.doi.org/10.1029/2006JB004655.

Brecher, A., 1976. Textural remanence: a new model of lunar rock magnetism. Earth Planet. Sci. Lett. 29, 131–145.

Brecher, A., 1977. Interrelationships between magnetization directions, magnetic fabric, and oriented petrographic features in lunar rocks. In: Proceedings of the 8th Lunar Science Conference, pp. 703–723.

Brecher, A., Leung, L., 1979. Ancient magnetic field determinations on selected chondritic meteorites. Phys. Earth Planet Inter. 20, 361–378.

Cisowski, S., Collinson, D., Runcorn, S., Stephenson, A., Fuller, M., 1983. A review of lunar paleointensity data and implications for the origin of lunar magnetism. In: Proceedings of the 13th Lunar Planetary Science Conference, pp. A691–A704.

Collinson, D., 1983. Methods in Rock Magnetism and Paleomagnetism. Chapman and Hall, New York, NY.

Cournede, C., Gattacceca, J., Rochette, P., 2012. Magnetic study of large Apollo samples: possible evidence for an ancient centered dipolar field on the Moon. Earth Planet Sci. Lett. 331-332, 31–42.

Dunlop, D., Ozdemir, O., 1997. Rock Magnetism: Fundamentals and Frontiers. Cambridge, UK.

Dunlop, D.J., 2002a. Theory and application of the Day plot (Mrs/Ms versus Hcr/Hc) - 2. Application to data for rocks, sediments, and soils. J. Geophys. Res., 107, http://dx.doi.org/10.1029/2001JB000487.

Dunlop, D.J., 2002b. Theory and application of the Day plot (Mrs/Ms versus Hcr/Hc)—1. Theoretical curves and tests using titanomagnetite data. J. Geophys. Res., 107, http://dx.doi.org/10.1029/2001JB000486.

Dwyer, C., Stevenson, D., Nimmo, F., 2011. A long-lived lunar dynamo driven by continuous mechanical stirring. Nature 479, 212–214.

Dyal, P., Parkin, C., Sonett, C., 1970. Apollo 12 Magnetometer: measurement of a steady magnetic field on the surface of the Moon. Science 169, 762–764.

Evensen, N., Murthy, V., Coscio, M., 1973. Rb-Sr ages of some mare basalts and the isotopic and trace element systematics in lunar fines. In: Proceedings of the 4th Lunar Science Confence, 1707-1724.

Fleischer, R., Hart, H., Comstock, G., Evwaraye, A., 1971. The particle track record of the ocean of storms. In: Proceedings of the 2nd Lunar Science Conference, pp. 2559–2568.

Fuller, M., Cisowski, S., 1987. Lunar paleomagnetism. Geomagnetism 2, 307–455.

Garcia, R., Gagnepain-Beyneix, J., Chevrot, S., Lognonne, P., 2010. The lunar core revealed by reflected seismic waves: constraints on the deep Moon seismic structure. EOS Transactions. AGU Fall Meeting, Abs. #GP43B.

Garrick-Bethell, I., Weiss, B., Shuster, D., Buz, J., 2009. Early lunar magnetism. Science 323, 356–359.

Garrick-Bethell, I., Weiss, B., Gattacceca, J., 2010. Pressure magnetization experiments and a common magnetization direction in mutually oriented samples of lunar troctolite 76535. In: Proceedings of the 73rd Annual Meteorological Society Meeting 5395.

Gattacceca, J., Rochette, P., Denise, M., Consolmagno, G., Folco, L., 2005. An impact origin for the foliation of chondrites. Earth Planet. Sci. Lett. 234, 351–368.

Gattacceca, J., Berthe, L., Boustie, M., Vadeboin, F., Rochette, P., De Resseguier, T., 2008. On the efficiency of shock magnetization processes. Phys. Earth. Planet. Inter. 166, 1–10.

Gattacceca, J., Boustie, M., Hood, L., Cuq-Lelandais, J.-P., Fuller, M., Bezaeva, N., de Resseguier, T., Berthe, L., 2010. Can the lunar crust be magnetized by shock: experimental groundtruth. Earth Planet. Sci. Lett. 299, 42–53.

Geiss, J., Eberhardt, P., Grogler, N., Guggisberg, S., Maurer, P., Stettler, A., 1977. Absolute time scale of lunar mare formation and filling. Philos. Trans. R. Soc. A 285, 151–158.

Guggisberg, S., Eberhardt, P., Geiss, J., Grogler, N., Stettler, A., 1979. Classification of the Apollo-11 mare basalts according to Ar39-Ar40 ages and petrological properties. In: Proceedings of the 10th Lunar Planetary Science Conference, pp. 1–39.

Hoffman, K., Banerjee, S., 1975. Magnetic "zig-zag" behavior in lunar rocks. Earth Planet. Sci. Lett. 25, 331–337.

Hood, L., Mitchell, D., Lin, R., Acuna, M., Binder, A., 1999. Initial measurements of the lunar induced magnetic dipole moment using Lunar Prospector magnetometer data. Geophys. Res. Lett. 26, 2327–2330.

Hood, L., Artemieva, N., 2008. Antipodal effects of lunar basin-forming impacts: initial 3D simulations and comparisons with observations. Icarus 193, 485–502.

Horn, P., Kirsten, T., Jessberger, E., 1975. Are there A 12 mare basalts younger than 3.1 b.y. Unsuccessful search for A 12 mare basalts with crystallization ages below 3.1 b.y. Meteoritics 10, 417–418.

Hu, S., Appel, E., Hoffmann, V., Schmahl, W.W., Wang, S., 1998. Gyromagnetic remanence acquired by greigite (Fe_3S_4) during static three-axis alternating field demagnetization. Geophys. J. Int. 134, 831–842.

Kirschvink, J., 1980. The least-squares line and plane and the analysis of palaeomagnetic data. Geophys. J. R. Astr. S 62, 699–718.

Kirschvink, J., Kopp, R., Raub, T., Baumgartner, C., Holt, J., 2008. Rapid, precise, and high-sensitivity acquisition of paleomagnetic and rock magnetic data: development of a low-noise automatic sample changing system for superconducting rock magnetometers. Geochem. Geophys. Geosyst. 9, 1–18.

Kirsten, T., Deubner, J., Horn, P., Kaneoka, I., Kiko, J., Schaeffer, O., Thio, S., 1972. The rare gas record of Apollo 14 and 15 samples. In: Proceedings of the 3rd Lunar Planetary Science Conference, pp. 1865–1889.

Konopliv, A., Binder, A., Hood, L., Kucinskas, A., Sjogren, W., Williams, J., 1998. Improved gravity field of the Moon from Lunar Prospector. Science 281, 1476–1480.

Kramer, F.E., Twedell, D.B., Walton, W.J.A., 1977. Apollo 11 Lunar Sample Information Catalogue. Nat. Aeronaut. Space Adm., Houston, TX.

Lawrence, K., Johnson, C., Tauxe, L., Gee, J., 2008. Lunar paleointensity measurements: implications for lunar magnetic evolution. Phys. Earth Planet. Inter. 168, 71–87.

Lawrence, K., Johnson, C., 2009. Magnetic characterization of lunar samples: back to basics. In: Proceedings of the 40th Lunar Planetary Science, p. 1433.

Le Bars, M., Wieczorek, M., Karatekin, O., Cebron, D., Laneuville, M., 2011. An impact-driven dynamo for the early Moon. Nature 479, 215–218.

Meyer, C., 2008. The Lunar Sample Compendium (online). 〈http://www-curator.jsc.nasa.gov/lunar/compendium.cfm〉.

Morrison, D.M., D.S., Heiken, G., Moore, H., 1973. Microcraters on lunar rocks. In: Proceedings of the 3rd Lunar Science Conference, pp. 2767–2791.

Nagata, T., Fisher, R., Schwerer, F., Fuller, M., Dunn, J., 1972. Summary of Rock Magnetism of Apollo 15 Lunar Materials, The Apollo 15 Lunar Samples. The Lunar Science Institute, Houston, pp. 442–445.

Nagata, T., Fisher, R., Schwerer, F., Fuller, M., Dunn, J., 1973. Magnetic properties and natural remanent magnetization of Apollo 15 and 16 lunar materials. In: Proceedings of the 4th Lunar Science Conference, pp. 3019–3043.

Pearce, G., Gose, W., Strangway, D., 1973. Magnetic studies on Apollo 15 and 16 lunar samples. In: Proceedings of the 4th Lunar Science Conference, pp. 3045–3076.

Pike, C., Roberts, A., Verosub, K., 1999. Characterizing interactions in fine magnetic particle systems using first order reversal curves. J. Appl. Phys. 85, 6660–6667.

Potter, D., 2011. Novel magnetic techniques for rapidly detecting palaeomagnetically important single-domain iron particles and obtaining directional palaeomagnetic data from "unoriented" lunar rock samples. Can. Aeronaut. Space J. 57, 12–23.

Pritchard, M., Stevenson, D., 2000. Thermal aspects of a lunar origin by giant impact. In: Canup, R., Righter, K. (Eds.), Origin of the Earth and Moon. University of Arizona Press, Tucson, pp. 179–196.

Runcorn, S.K, 1996. The formation of the lunar core. Geochim. Cosmochim. Acta 60, 1205–1208.

Shea, E., Weiss, B., Cassatta, W., Shuster, D., Tikoo, S., Gattacceca, J., Grove, T., Fuller, M., 2012. A long-lived lunar core dynamo. Science 335, 453–456.

Srnka, L., 1977. Spontaneous magnetic field generation in hypervelocity impacts. In: Proceedings of the 8th Lunar Planetary Science Conference, pp. 785–792.

Stegman, D., Jellinek, A., Zatman, S., Baumgardner, J., Richards, M., 2003. An early lunar dynamo driven by thermochemical mantle convection. Nature 421, 143–146.

Stephenson, A., Collinson, D., 1974. Lunar magnetic field paleointensities determined by an anhysteretic remanent magnetization method. Earth Planet. Sci. Lett. 23, 220–228.

Stephenson, A., 1980. A gyroremanent magnetisation in anisotropic magnetic material. Nature 284, 49–51.

Stephenson, A., Sadikun, S., Potter, D., 1986. A theoretical and experimental comparison of the anisotropies of magnetic susceptibility and remanence in rocks and minerals. Geophys. J. R. Astron. Soc. 84, 185–200.

Stephenson, A., 1993. Three-axis static alternating field demagnetization of rocks and the identification of natural remanent magnetization, gyroremanent magnetization, and anisotropy. J. Geophys. Res. 98, 373–381.

Tanaka, H., Kono, M., 1984. Analysis of the Thelliers' method of paleointensity determination 2: Applicability to high and low magnetic fields. J. Geomagn. Geoelectr. 36, 285–297.
Warner, J., 1970. Apollo 12 Lunar Sample Information Catalog. Nat. Aeronaut. Space Adm., Washington, DC.
Weber, R., Lin, P., Garnero, E., Williams, Q., Lognonne, P., 2011. Seismic detection of the lunar core. Science 331, 309–312.
Weiss, B., Gattacceca, J., Stanley, S., Rochette, P., Christensen, U., 2010. Paleomagnetic records of meteorites and early planetesimal differentiation. Space Sci. Rev. 152, 341–390.
Wieczorek, M., Jolliff, B., Khan, A., Pritchard, M., Weiss, B., 2006. The constitution and structure of the lunar interior. Rev. Mineral. Geochem. 60, 221–364.
Wieczorek, M., Weiss, B., Stewart, S., 2012. An impactor origin for lunar magnetic anomalies. Science 335, 1212–1215.